Evaluation of penetration resistance, vertical bearing capacity and pull-out resistance of small diameter spiral piles subjected to positive and negative alternating loads in unsaturated sandy ground

F. Shah
Graduate student, Faculty of Engineering, Hokkaido University, Sapporo, Japan

K. Isobe
Associate Professor, Faculty of Engineering, Hokkaido University, Sapporo, Japan

T. Eki
Graduate student, Faculty of Engineering, Hokkaido University, Sapporo, Japan

K. Kawai
Undergraduate student, Faculty of Engineering, Hokkaido University, Sapporo, Japan

ABSTRACT

The growing demand for renewable energy has led to a notable increase in the construction of solar power equipment, often situated on cost-effective land with less-than-ideal ground conditions. While conventional concrete spread footings are commonly employed for solar power generation, spiral piles have become popular for construction on soft ground due to their robust resistance against vertical loads. They are also utilized to reinforce sloped ground, leveraging their rotational penetration to enhance lateral support. However, the design of spiral piles often errs on the side of caution, neglecting to consider the integration effect. Furthermore, previous studies predominantly focused on dry sand and monotonic loading, lacking real-world applicability. In response to these gaps in understanding, an experimental investigation was undertaken, specifically targeting small-diameter spiral piles. The investigation delved into penetration resistance, vertical bearing capacity, and pull-out resistance in unsaturated sandy soil under cyclic loading conditions. The study revealed unique mechanisms at play in unsaturated sandy soil, showcasing an increase in pull-out resistance attributed to apparent cohesive forces arising from suction within the soil. Additionally, it was confirmed that the cyclic loading-induced gap between the spiral pile and the ground is maintained by apparent adhesive forces in unsaturated sandy soil. The findings highlighted that displacements are necessary to eliminate the gap and allow for the reapplication of circumferential resistance forces.

Keywords: Spiral piles, Unsaturated sand, Cyclic loading, Apparent cohesion

1. Introduction

In recent years, the demand for renewable energy has driven a surge in the construction of solar power generation equipment. This trend has led to an increase in construction on cost-effective land with less-than-ideal ground conditions. While conventional concrete spread footings are a standard approach for solar power generation equipment, the development of foundation types utilizing small-diameter and short-length steel pipe piles, spiral piles, and diagonal piles has gained momentum in addressing soft ground conditions (Hirata et al., 2005; Araki, 2013; Sato et al., 2015; Nakagawa et al., 2018; Tamboura et al., 2022).

Among these alternatives, spiral piles stand out for their notable resistance to vertical loads, making them particularly useful for construction on soft ground and for reinforcing slopes due to their rotational penetration,

which enhances lateral support. Recently, spiral piles have found applications in the construction of soundproof wall foundation structures on embankments and the development of platform door foundation structures in conjunction with high-strength fiber-reinforced floor slabs.

However, practical designs often err on the side of caution when considering spiral piles, neglecting to account for their integration effect. Moreover, previous studies predominantly used dry sand, providing limited insights under more realistic or strictly controlled conditions such as cohesive or unsaturated ground. Therefore, a more rational evaluation and design of the bearing capacity characteristics of spiral piles under actual ground conditions can potentially expand their application.

In this study, we experimentally investigated the penetration resistance, vertical bearing capacity, and pull-out resistance of small-diameter spiral piles in unsaturated sandy soil under cyclic loading. A comprehensive assessment was conducted by comparing the vertical bearing capacity and pull-out resistance mechanisms of the spiral pile with those of a normal pile. This comparison considered both saturated and unsaturated sandy soil under cyclic loading conditions. However, because these experiments are conducted under gravitational conditions, caution is necessary when applying the results to real scale structures.

2. Outline of model test
2.1. Model piles

In this set of experiments, two types of piles underwent examination: the conventional pile (NP12) and the spiral pile (SP15). The conventional pile is characterized as a straight pile with a diameter (D_P) of 12 mm. In contrast, the spiral pile also features a 12 mm pile diameter (D_P) but is distinguished by the inclusion of a spiral blade with a wing diameter (D_W) of 25 mm (see **Fig. 1**). This spiral blade is securely attached to the circumferential surface of the straight pile using adhesive. The spiral blade follows a right winding direction with a pitch of 14 mm and covers the entire pile, excluding the tip. The effective surface area and effective bearing area of the spiral pile were determined under the assumption of a 25 mm diameter, resulting in a conservative estimation of the end bearing capacity. However, it is recognized that the actual effective diameter likely falls within the range

of 12 mm to 25 mm. Further investigation is needed to accurately assess the effective bearing area for the spiral pile. Nevertheless, for safety reasons at this stage, the conservative estimation approach is deemed appropriate.

To measure axial force, two strain gauges (SG) per cross-section were attached to the inner surface of each pile at five locations as shown in **Fig. 1**. The locations for attaching strain gauges on the spiral pile were the same as those for NP12. **Table 1** provides a summary of the essential properties of both types of piles.
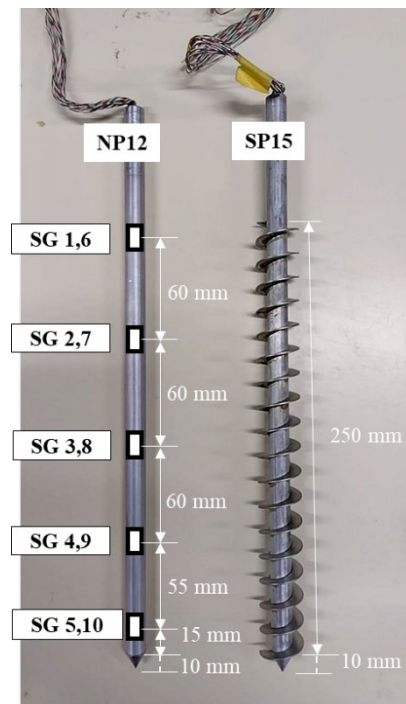
Fig. 1 Model piles

Table 1. Model piles data

	NP12	SP15
Mass (kg)	0.056	0.096
Total length (mm)	313	313
Effective length (mm)	260	260
Pile diameter D_P (mm)	12	12
Wing diameter D_W (mm)	-	25
Effective surface area (mm²)	9769.8	20410
Effective base area (mm²)	113.04	490.625
Wing pitch p_w (mm)	-	14
Young's modulus (GPa)	69.1	70.8

2.2. Model ground preparation

The experimental setup utilized a cylindrical soil chamber depicted in **Fig. 2** and **Fig. 3**, featuring a diameter

of 300 mm and a depth of 640 mm. Silica sand No. 7 served as the model ground material, with a total height of 360 mm achieved through 12 layers, each 30 mm in height. To attain a relative density of 45%, pluviation in air from a height of 630 mm was employed. The physical properties of the silica sand can be found in **Table 2**.

To establish saturated conditions, water was introduced into the tank from the bottom, promoting infiltration through the model ground. The water level within the ground model was carefully monitored. Once the water level reached the surface of the ground, the pouring of water was stopped, and the water level was maintained for an adequate duration to achieve equilibrium. This ensured thorough water permeation throughout the model ground, confirming the establishment of saturated conditions.

To create unsaturated conditions, the soil was initially saturated, and water was subsequently drained by applying air pressure from the top of the soil down to the bottom of the tank. This method effectively transitioned the entire model ground from a saturated to an unsaturated state. To determine the degree of saturation, five pore water pressure gauges (WP) were installed in the soil tank (see **Fig. 3**) to measure the pressure heads. The pressure heads during the test were measured and are presented in **Table 3**. The volumetric water content was estimated from the soil water characteristic curve (SWCC) shown in **Fig. 4a**, which was obtained using the suction head method (hydraulic head method). The degree of saturation values was then estimated from the corresponding suction values at various depths using **Fig. 4b.**

Table 2.   Silica sand No. 7 properties

Physical property	Silica sand
ρ_s (g/cm^3)	2.67
ρ_{dmax} (g/cm^3)	1.60
ρ_{dmin} (g/cm^3)	1.25

2.3. Penetration of model piles

The normal pile was initially dropped from a height slightly above the level of the model ground, aiming to achieve penetration into the ground solely through its own

weight. However, the pile did not reach the specified depth of 260 mm through free fall alone. Consequently, a press-in technique was employed, involving the application of additional loads to facilitate the pile's installation to the desired depth. In a step-wise procedure, an additional load of 500 grams was incrementally placed on the top of the rotary bracket, and the corresponding penetration of the pile was recorded (see **Fig. 3**).
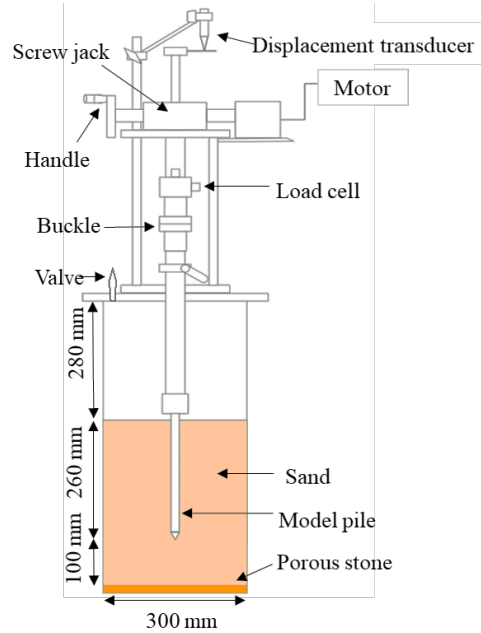
Fig. 2 Cylindrical soil chamber with loading device
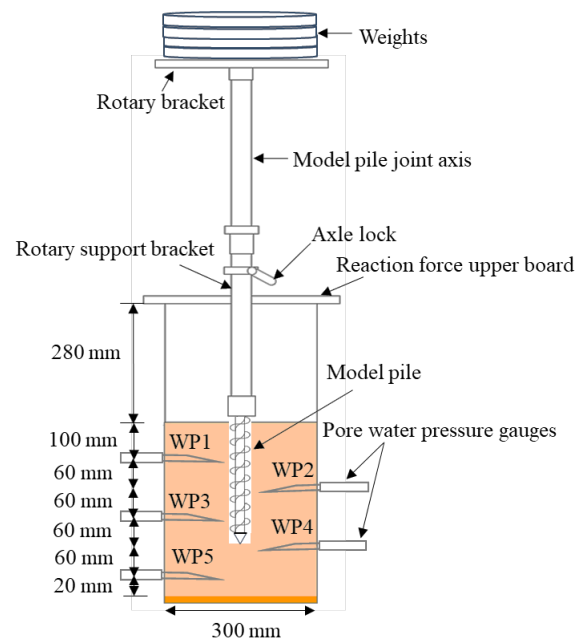
Fig. 3 Cylindrical soil chamber with penetration device
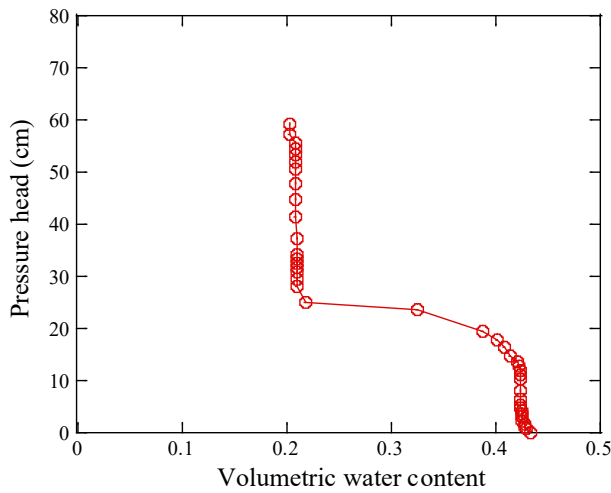
(a) Volumetric water content vs pressure head (cm)
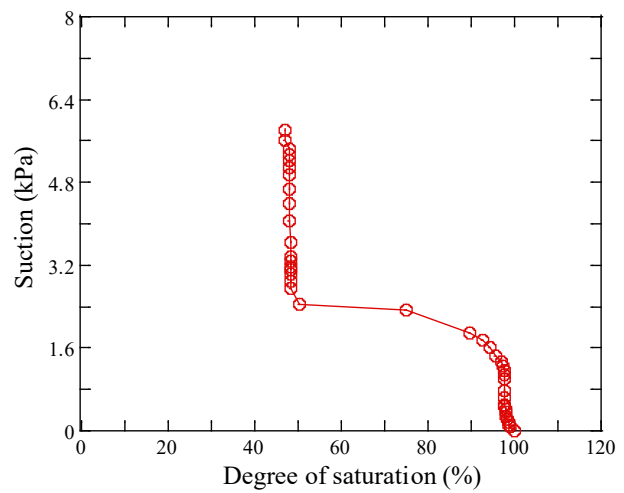
(b) Degree of saturation (%) vs suction (kPa)

Fig. 4 Soil water characteristics curve (SWCC)

Table 3.   Pore water pressure heads for NP12 and SP15

Pressure head	WP1 (kPa)	WP2 (kPa)	WP3 (kPa)	WP4 (kPa)	WP5 (kPa)
NP12	-3.22	-2.31	-1.39	-1.10	-0.74
SP15	-2.05	-1.82	-0.69	-0.63	-0.15

Once the pile reached 80% of the target penetration depth, a loading device (as depicted in **Fig. 2**) was attached to the pile to apply controlled displacement, ensuring that the pile did not exceed the prescribed total penetration depth of 260 mm.

For the screw pile, a similar mechanism was employed, but with an additional step. After the initial free fall, the pile was manually rotated through the rotary bracket during penetration, as illustrated in **Fig. 3**. Simultaneously, a weight was positioned on the rotary bracket to maintain a consistent amount of penetration per rotation, matching the pitch of the spiral pile. This approach was adopted to minimize soil disturbance.

2.4. Loading procedure

The loading device illustrated in **Fig. 2** was affixed to the pile post-installation. Throughout this sequence of loading tests, it was assumed that the pile experiences allowable bearing capacity conditions before progressing to ultimate bearing capacity. The latter is deemed achieved when vertical or lateral displacement reaches 10% of the pile diameter at the loading point.

To simulate the allowable bearing capacity scenario, the piles initially underwent cyclic loading until a displacement of 2% of the pile diameter was reached, both in the push-in and pull-out directions. This procedure was iterated for six loading cycles, maintaining a controlled loading speed of 0.5 mm/min. Subsequently, the piles were subjected to additional loading to attain the ultimate bearing capacity condition, characterized by a vertical displacement of 10% of the pile diameter in both the push-in and pull-out directions. This subsequent phase encompassed an additional six loading cycles, conducted at an elevated loading speed of 2.5 mm/min, as the loading speed effect was considered almost negligible in these tests.

3. Test results

3.1. Penetration resistance

Fig. 5 and **Fig. 6** depict the relationship between penetration resistance and the percentage rate of displacement to the target depth (260 mm) for both the normal pile and the spiral pile under saturated and unsaturated conditions. In both scenarios, the spiral pile, despite its larger diameter of 25 mm, exhibits lower penetration resistance compared to the normal pile with a diameter of 12 mm. This observation validates that the rotary penetration of the spiral pile, where the amount of penetration per rotation aligns with the pitch of the spiral, can effectively minimize the penetration resistance of the

spiral pile.

The normal pile, mainly relying on tip resistance, shows significantly high penetration resistance at shallow depths when compared to the spiral pile (see **Fig. 6**). At shallower depth the skin resistance of the spiral is small however, as the depth of penetration increases, the penetration resistance of the spiral pile also increases in correlation with the rising skin resistance. Nevertheless, the spiral pile shows overall less penetration resistance than the normal pile. Additionally, in unsaturated conditions, both piles exhibit high penetration resistance compared to saturated conditions. This increased resistance is attributed to the increased suction and cohesion of sandy soil in unsaturated conditions, where greater moisture tension causes soil particles to bind more tightly, leading to a more substantial overall resistance to pile penetration.
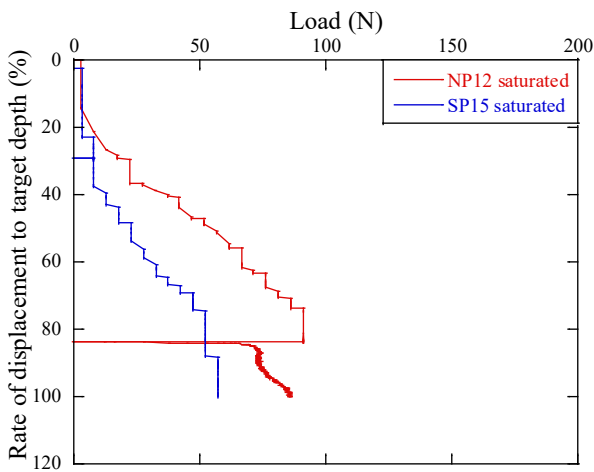
Fig. 5 Penetration resistance vs rate of displacement in a saturated condition
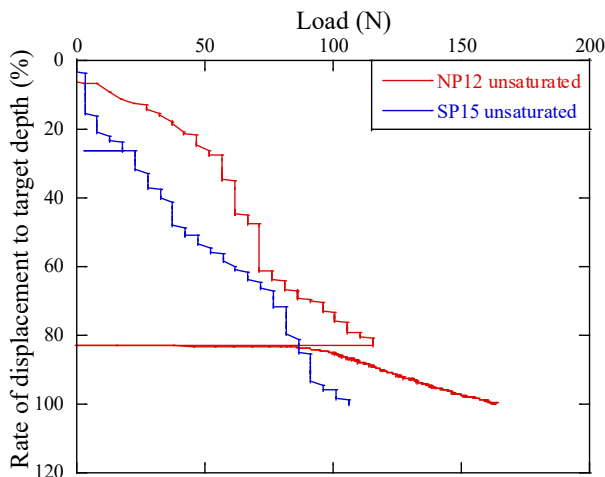
Fig. 6 Penetration resistance vs rate of displacement in unsaturated condition

3.2. Loading test results

Fig. 7 and **Fig. 8** illustrate the relationship between load and percentage displacement normalized by the pile diameter. In both saturated and unsaturated conditions, the spiral pile consistently exhibits significantly higher vertical bearing capacity compared to the normal pile, approximately five times higher in saturated conditions and six times higher in unsaturated conditions (see **Fig. 7** and **Fig. 8**).

The increased vertical-bearing capacity of the spiral pile is attributed to the enhanced skin friction generated by its unique spiral configuration. The spiral configuration of the pile introduces additional helical surfaces, leading to increased contact area with the surrounding soil. This, in turn, generates higher skin friction between the pile and the soil, contributing to enhanced load-bearing capacity. While the spiral pile does not show a substantial increase in pullout-bearing capacity compared to its vertical-bearing capacity, but it still outperforms the normal pile in pullout capacity. In both saturated and unsaturated conditions, the spiral pile consistently demonstrates a notably higher pullout bearing capacity when compared to the normal pile. Specifically, the pullout capacity of the spiral pile is approximately three times higher in saturated conditions and six times higher in unsaturated conditions. This increase can be attributed to the higher skin friction provided by the helical surfaces of the spiral shape (refer to **Fig.11** and **Fig. 12**).

The normal pile exhibits cyclic degradation in vertical-bearing capacity under both saturated and unsaturated conditions, as indicated in **Fig. 7a** and **Fig. 8a**. The degradation is more pronounced in unsaturated conditions, primarily attributed to the decrease in tip resistance during cyclic loading (refer to **Fig 10a**). This trend is similarly observed in the pull-out bearing capacity of the normal pile. Conversely, the spiral pile demonstrates a less noticeable degradation in vertical-bearing capacity in saturated conditions compared to unsaturated conditions (refer to **Fig. 7b** and **Fig. 8b**). In unsaturated conditions, the load-bearing capacity of the spiral pile experiences a significant degradation after the first cycle of each cyclic loading due to degradation of tip resistance (see **Fig 10b**.). This reduction in tip resistance

is attributed to the cyclic

resistance. However, it is recognized that the actual

(a) NP12

(b) SP15
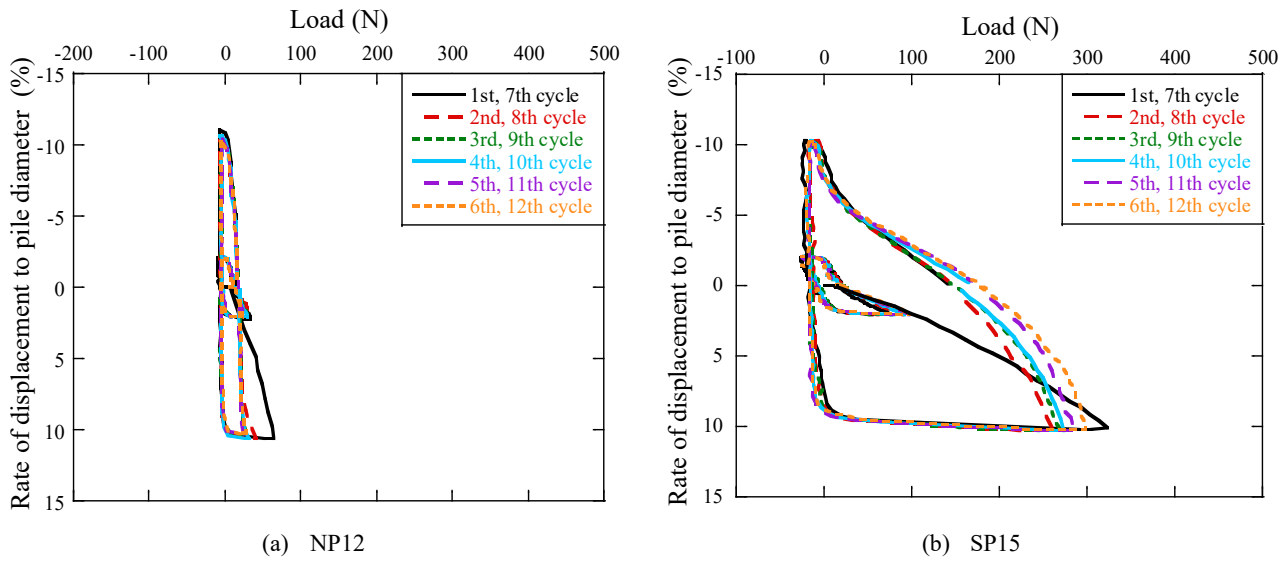
Fig. 7 Load vs displacement ratio in saturated condition

(a) NP12

(b) SP15
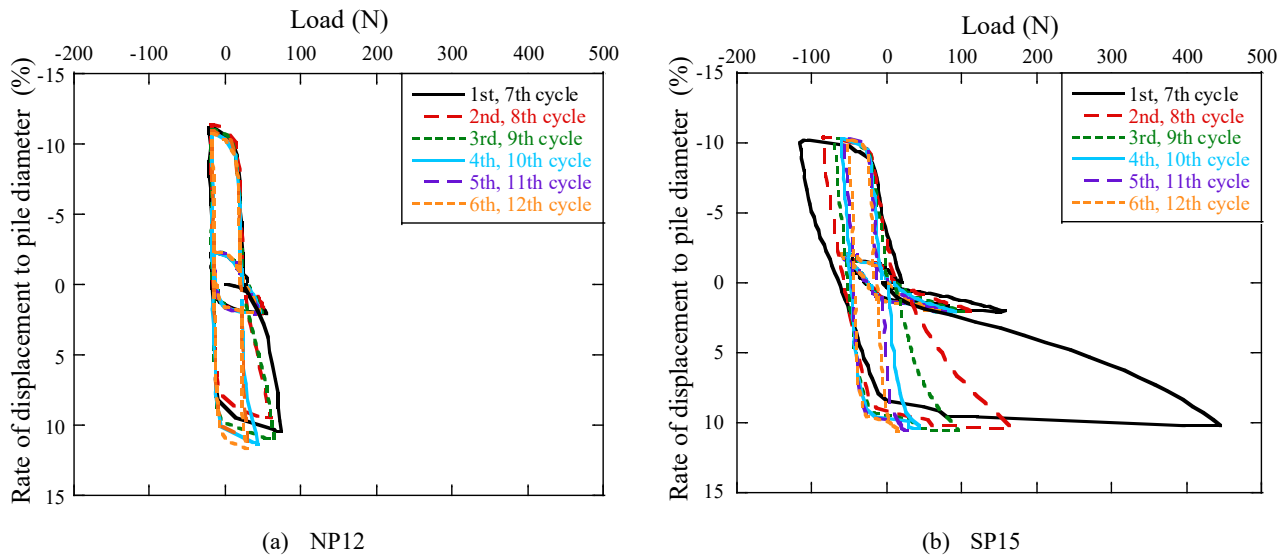
Fig. 8 Load vs displacement ratio in unsaturated conditions

loading-induced gap between the spiral pile and the ground, maintained by apparent adhesive forces in unsaturated sandy soil. The findings highlighted that further displacements are necessary to eliminate the gap and allow for the reapplication of circumferential resistance forces. A similar degradation pattern is also observed in the pull-out bearing capacity of the spiral pile.

Fig. 9 and **Fig. 10** illustrate the relationship between tip resistance and percentage displacement normalized by the pile diameter. The effective bearing area of the spiral pile was determined under the assumption of a 25 mm diameter, resulting in a conservative estimation of the tip

effective diameter likely falls within the range of 12 mm to 25 mm. Further investigation is needed to accurately assess the effective bearing area for the spiral pile. Nevertheless, for safety reasons at this stage, the conservative estimation approach is deemed appropriate. The tip resistance of the normal pile in unsaturated conditions is higher than that in saturated conditions. The normal pile shows degradation in tip resistance in both saturated and unsaturated conditions under cyclic loading. On the other hand, the spiral pile shows a different behavior in both saturated and unsaturated conditions. The tip resistance of the spiral pile in saturated

(a) NP12   (b) SP15
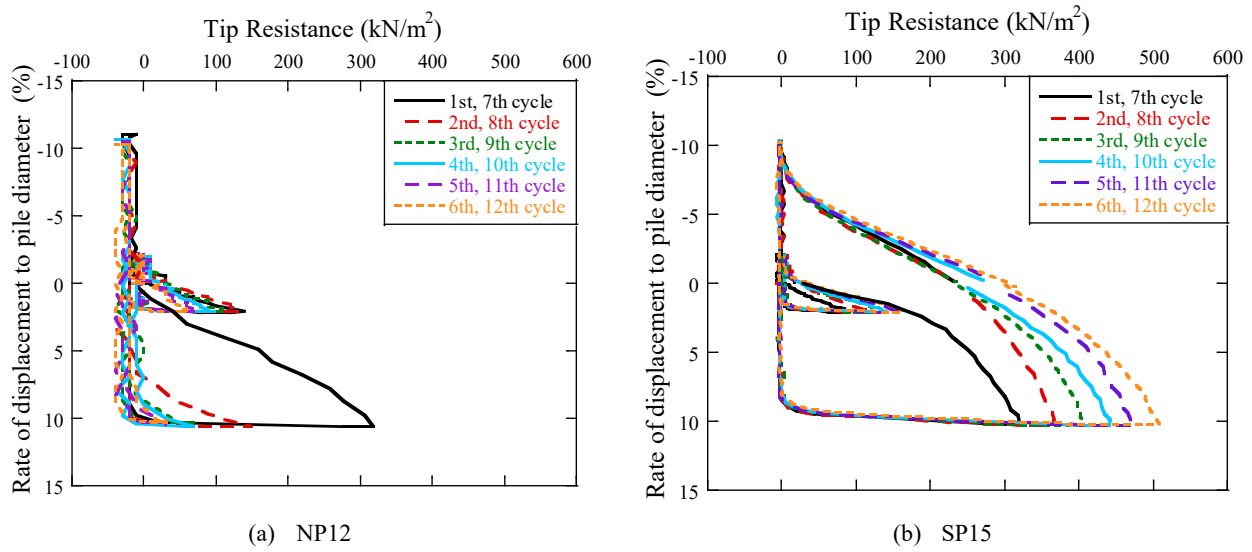
Fig. 9 Tip resistance vs displacement ratio in saturated conditions

(a) NP12   (b) SP15
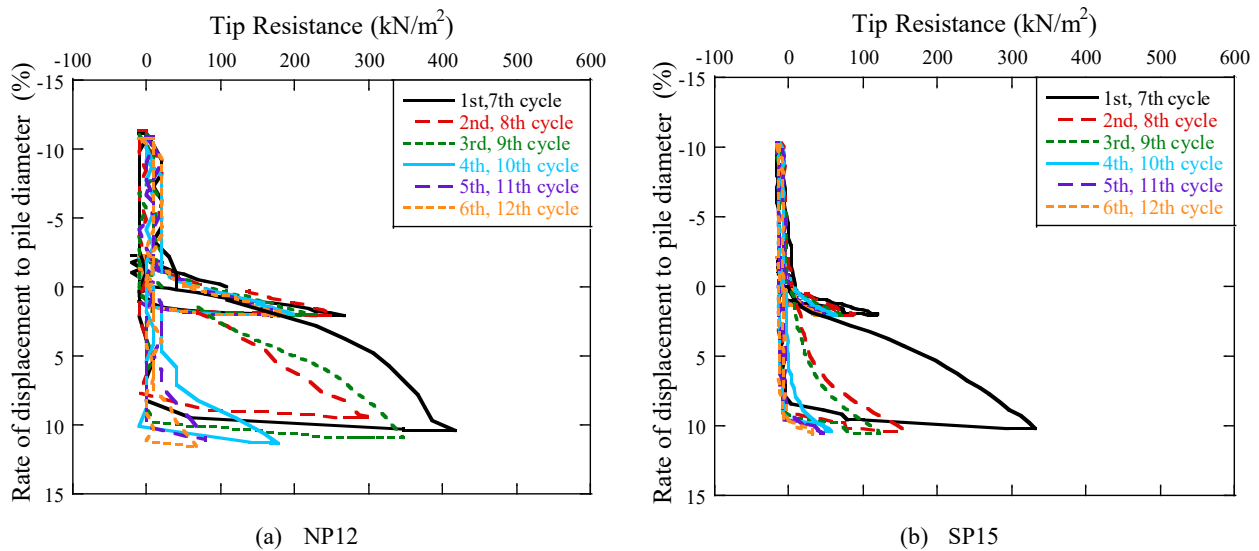
Fig. 10 Tip resistance vs displacement ratio in unsaturated conditions

conditions exhibits an increase as the number of loading cycles in both loading sequences increases. Cyclic loading in saturated conditions induces a dynamic interaction between the spiral pile and the surrounding soil. The repeated loading and unloading cycles can lead to the densification and compaction of the soil under the tip of the spiral pile. As the soil particles rearrange and water is expelled from the voids, the soil becomes more compacted, increasing tip resistance (see **Fig 9b**). The tip resistance of the spiral pile degrades in unsaturated conditions after the 1st cycle of each loading sequence as shown in **Fig. 10b**. This decrease in the tip resistance is indicative of a cyclic-loading-induced gap between the pile and the soil.

Following the first cycle in the second loading sequence, the soil suction maintains this gap, allowing the pile to move freely with minimal tip resistance. As a result, a larger displacement is required to activate the tip resistance again, confirming the cyclic-loading-induced gap as a significant factor influencing tip resistance behavior in unsaturated conditions.

Fig. 11 and **Fig. 12** depict the relationship between skin frictional resistance and the percentage displacement normalized by the pile diameter. The spiral pile consistently exhibits notably higher skin friction compared to the normal pile. In saturated conditions, the

(a) NP12   (b) SP15
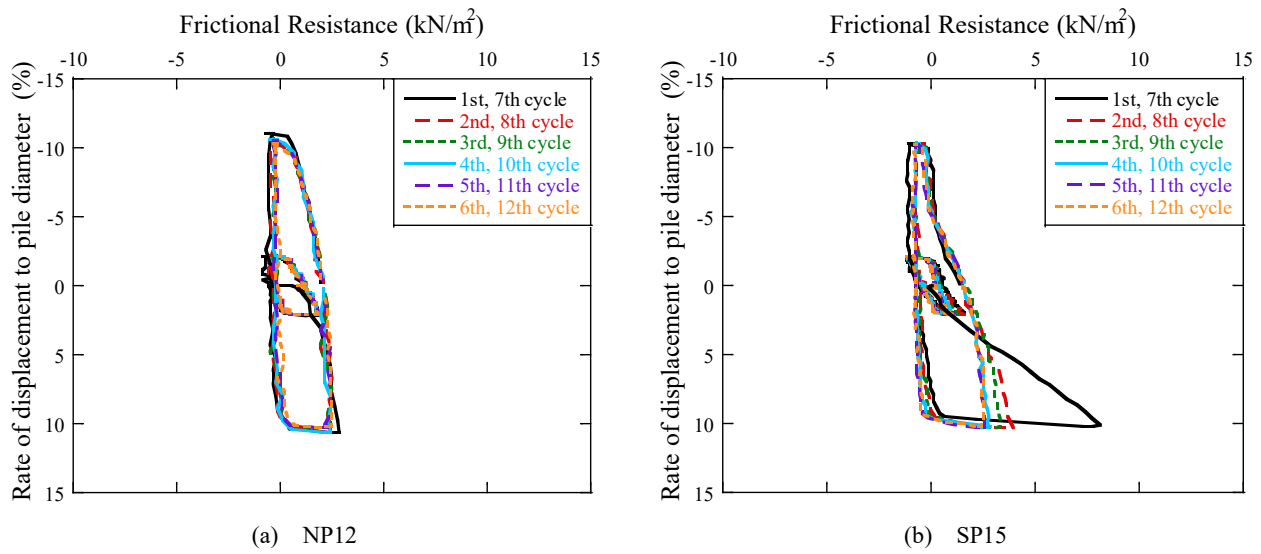
Fig. 11 Skin resistance vs displacement ratio in saturated conditions

(a) NP12   (b) SP15
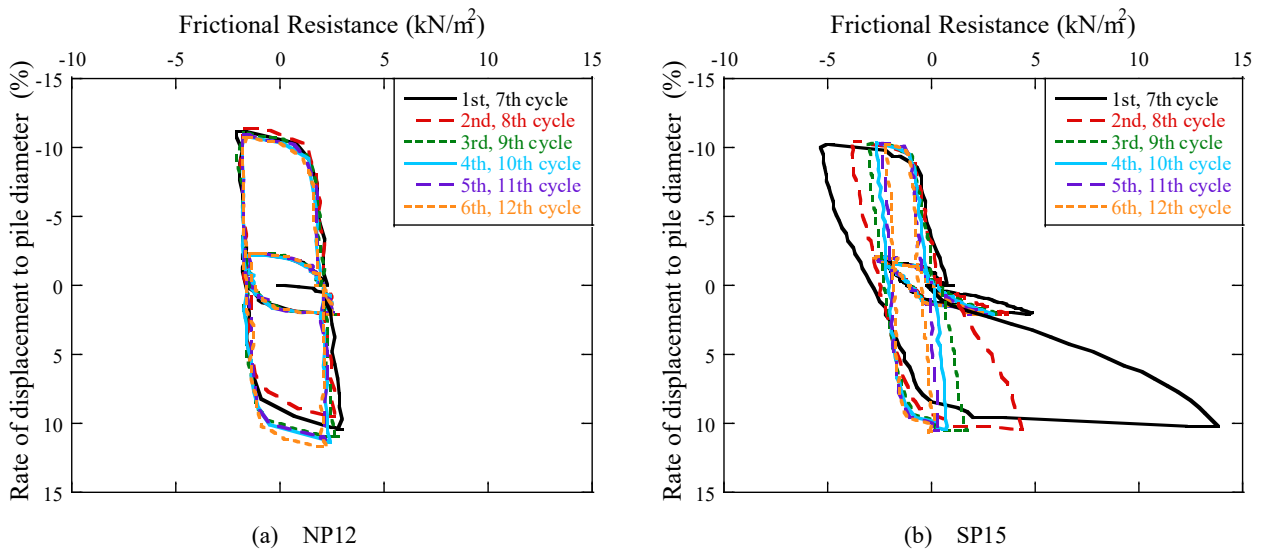
Fig. 12 Frictional resistance vs displacement ratio in unsaturated conditions

skin friction in compression for the spiral pile is approximately three times greater than that of the normal pile, and in unsaturated conditions, it is around five times higher. Similarly, in pullout conditions, the skin friction of the spiral pile is approximately two times greater than that of the normal pile in both saturated and unsaturated conditions. This observed increase in skin friction is a characteristic feature attributed to the spiral configuration. The helical surfaces introduced by the spiral configuration result in a larger contact area with the surrounding soil, generating higher skin friction and contributing to an overall enhanced load-bearing capacity (Wada et al., 2017).

The skin friction of the normal pile in saturated conditions remains consistent without significant degradation, following the same loading path in each cycle. In unsaturated conditions, particularly during the second loading sequence, the normal pile displays minimal degradation of skin friction in both compression and pullout loading tests. Unlike the normal pile, the spiral pile exhibits a more noticeable degradation in skin friction with an increase in the number of loading cycles, especially in unsaturated conditions. This decrease in skin friction suggests the presence of a cyclic-loading-induced gap between the pile and the soil. In saturated conditions, the skin friction of the spiral pile degrades after the first

cycle of the second loading sequence until the fourth cycle. After the fourth cycle, the skin friction stabilizes, indicating no further degradation. The pile maintains some level of skin friction thereafter. However, in unsaturated conditions, the spiral pile demonstrates a minimal amount of skin friction after the fourth cycle of the second loading sequence, confirming the unrestricted movement of the pile. This observed behavior is attributed to the gap maintained by soil suction, allowing the pile to move freely with almost negligible skin friction. A similar pattern is also evident in the pull-out loading condition of the spiral pile

4. Conclusions

The following conclusions are obtained.

1) The spiral pile, despite its larger diameter, exhibits lower penetration resistance compared to the normal pile. This observation validates that the rotary penetration of the spiral pile, where the amount of penetration per rotation aligns with the pitch of the spiral, can effectively minimize the penetration resistance of the spiral pile.

2) The normal pile, mainly relying on tip resistance, shows significantly high penetration resistance at shallow depths in unsaturated conditions when compared to the spiral pile. The spiral pile experiences lower resistance due to reduced skin friction at shallower depth.

3) The spiral pile demonstrates a notably higher vertical bearing capacity than the normal pile. The increased bearing capacity of the spiral pile is attributed to the enhanced skin friction generated by its unique spiral configuration.

4) The spiral pile does not show a substantial increase in pullout-bearing capacity compared to its vertical-bearing capacity; it still outperforms the normal pile in pullout capacity. This increase can be attributed to the higher skin friction provided by the helical surfaces of the spiral shape.

5) The normal pile exhibits cyclic degradation in vertical-bearing capacity under both saturated and unsaturated conditions. The degradation is more pronounced in unsaturated conditions, primarily attributed to the decrease in tip resistance during cyclic loading.

6) The spiral pile in unsaturated conditions, the load-bearing capacity of the spiral pile experiences a significant degradation due to the degradation of tip resistance. This reduction in tip resistance is attributed to the cyclic loading-induced gap between the spiral pile and the ground, maintained by apparent adhesive forces in unsaturated sandy soil. The findings highlighted that further displacements are necessary to eliminate the gap and allow for the reapplication of circumferential resistance forces.

The tip resistance of the spiral pile in saturated conditions demonstrates an increase with the number of cycles without degradation. In light of these findings, the authors express the intention to conduct future tests to validate and confirm the obtained results.

References

Araki, K., 2013. Simplified foundation method subject to small-scale structure "PIN FOUNDATION METHOD". The Japanese Geotechnical Society. Vol. 61, No. 8, pp. 32-33 (in Japanese).

Hirata, A., Kokaji, S. and Goto, T., 2005. Study on the estimation of the axial resistance of spiral bar based on interaction with ground. Shigen-to-Sozai, Vol. 121, pp. 370-377 (in Japanese).

Nakagawa, S., Yamauchi, R., Isobe, K., and Tomisawa, K., 2018. Evaluation of bearing capacity of a small-diameter spiral pile subjected to combined load using model tests. Proceedings of the 1st international conference on press-in engineering, Kochi. pp. 117-124. https://doi.org/10.50876/icpe.1.0_117

Sato, T., Harada, T., Iwasaki, N., Hayashi, S. and Ohtani, J., 2015. Effect of shaft rotation of spiral piles under its installation on vertical bearing capacity. Japanese Geotechnical Journal, Vol. 10, No. 2, pp. 253-265 (in Japanese).

Tamboura, H.H., Yamauchi, R., and Isobe, K., 2022. Bearing capacity evaluation of small-diameter spiral piles in soft ground subjected to combined loads. Soils and Foundations. Vol. 62, No. 5. https://doi.org/10.1016/j.sandf.2022.101204

Wada, M., Tokimatsu, K., Maruyama, S., and Sawaishi, M., 2017. Effects of cyclic vertical loading on bearing and pullout capacities of piles with continuous helix wing. Soils and Foundations, Vol. 57, No. 01, pp 141-153. ISSN 0038-0806. https://doi.org/10.1016/j.sandf.2017.01.010